Preprint Cambridge Centre for Computational Chemical Engineering ISSN 1473 – 4273

A hybrid particle-number and particle model for efficient solution of population balance equations

Astrid Boje[1], Jethro Akroyd[1], Markus Kraft[1,2,3]

released: 3 October 2018

[1] Department of Chemical Engineering
and Biotechnology
University of Cambridge
West Cambridge Site
Philippa Fawcett Drive
Cambridge, CB3 0AS
United Kingdom
E-mail: mk306@cam.ac.uk

[2] Cambridge Centre for Advanced Research
and Education in Singapore (CARES)
CREATE Tower, 1 CREATE Way
138602
Singapore

[3] School of Chemical and
Biomedical Engineering
Nanyang Technological University
62 Nanyang Drive
Singapore, 637459

Preprint No. 211

Keywords: hybrid method, particle model, particle-number model, high rate, particle processes, population balance

Edited by
Computational Modelling Group
Department of Chemical Engineering and Biotechnology
University of Cambridge
West Site, Philippa Fawcett Drive
Cambridge CB3 0AS
United Kingdom

Fax: + 44 (0)1223 334796
E-Mail: c4e@cam.ac.uk
World Wide Web: http://como.cheng.cam.ac.uk/

Abstract

This work presents a hybrid particle-number and particle model to improve efficiency in solving population balance equations for type spaces spanning spherical and aggregate particles. The particle-number model tracks simpler, spherical particles cheaply by storing only the number of particles with a given one-dimensional internal coordinate, while the particle model allows resolution of the detailed aggregate structure that occurs due to collision and coagulation between particles by storing distinct computational entries for each particle. This approach is exact if primary particles are defined by their monomer count and the particle-number model increments in single monomers. A stochastic method is used to solve the population balance equations for the combined type space. The hybrid method works well for large ensembles ($> 2^{12}$ particles) with a detailed particle model, where performing a finite number of particle-number updates is demonstrated to be 40-50% cheaper than updating an equivalent ensemble of discrete particles. These savings can be traded for a larger sample volume to increase the resolution in the particle size distribution or more repeat runs to reduce the total error. Run time improvements are curtailed at very high surface growth and coagulation rates due to the fixed cost of growth updates on the large aggregates formed; however, the hybrid method is still attractive in this case as its primary purpose is to reduce error by preventing saturation of the ensemble with simple particles at high inception rates.

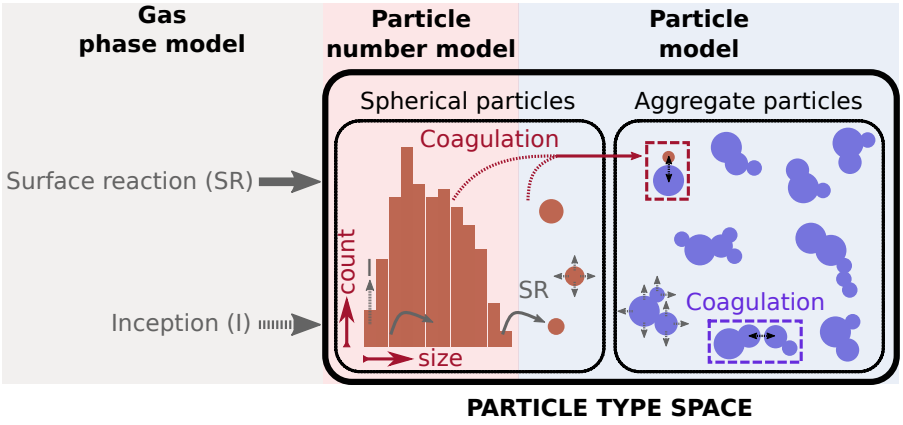

Highlights

- The hybrid type space (particle-number/particle) model allows efficient representation of small, spherical particles while preserving detailed structural information for larger particles and aggregates.
- The population balance equations for both type spaces are advanced using a stochastic method; the method is exact if primary particles are integer multiples of a monomer size.
- Speed-up of 40-50% is obtained for large ensembles, with best performance for systems with many small particles, especially if particle updates are expensive.
- With the proposed method, smaller ensembles are required to achieve a given level of accuracy and the chance of contractions due to ensemble flooding is reduced.

Contents

1 Introduction

The dynamics of particle formation and growth are of interest across a wide range of systems from flame synthesis of nanoparticles [28, 39] to crystallisation [33]. The evolution of a particle system through time and space can be described by its population balance equation (PBE), an integro-differential equation which describes changes in the internal coordinates of the particles (e.g. mass, surface area, chemical composition and structure) due to processes such as inception, collision, surface reaction or condensation, and fragmentation. The complexity of real systems precludes analytical solutions; thus numerical methods have been developed. Numerical solutions require a model for the particle type space and a method for solving the PBE.

The particle type space is typically high dimensional, with each particle described by up to thousands of internal coordinates which correspond to the diversity of morphologies and surface chemistries that can be formed [13]. The simplest type space model is a spherical particle model, which represents particles as spheres of constant composition and density; thus only a one dimensional type space is required. This assumes that lasting collision (i.e. coagulation) events are followed by instantaneous coalescence to a larger spherical particle [32]. More detail is incorporated into surface area and volume models [45], where these properties are added for coagulating particles. This allows more structural information to be tracked; however, these models require adaptations to deal with processes such as surface reaction and sintering (e.g. a fractal dimension is assumed).

The most detailed particle models are primary particle models. These resolve the connectivity of "primary particles" (particles formed by inception) following coagulation events and describe particle structure e.g. shared surface area and centre-to-centre distance between particles [18]. Detailed particle models have been used to study synthesis of soot [6, 35, 46], SiO_2 [34, 36], silicon [25] and TiO_2 [4, 18, 42]. Detailed particle models have been shown to provide important additional information when the particle system is polydisperse or the coagulation and sintering timescales are similar [24].

The numerical solution of the PBE becomes more challenging with increasing type space complexity. Low dimensional type spaces allow direct integration of the ordinary differential equations (ODE) through transport of the moments of the particle size distribution (PSD) or discretization.

The method of moments (MOM) approach solves finitely many moments of the particle size distribution by multiplying the PBE by k^{th} powers of a property and integrating over the type space. This approach is computationally efficient, although closure problems exist for coagulation kernels involving fractional or negative moments and processes requiring the point-wise particle concentrations (shrinkage). Closure issues are treated by interpolation e.g. MOMIC [2, 9, 10, 20] or quadrature e.g. QMOM [22, 23], DQMOM [1, 21]. The moment projection method has been proposed to handle shrinkage problems [44].

Sectional methods are a popular choice of ODE-based method. These discretize the PSD into sections/bins within which the PSD is modelled either with step functions or polynomials. A number of adaptations have been proposed to e.g. conserve mass and particle number [11], handle discontinuities in the number distribution and numerical diffusion

due to surface reaction [14–16], and treat sintering [38]. However, sectional methods must approximate properties of the PSD within the discretized sections, are expensive compared with MOM, and higher order variants can suffer from stability issues [13].

Stochastic (Monte Carlo) methods solve the PBE by performing events probabilistically on a finite ensemble of computational particles which can have arbitrarily many internal coordinates. Monte Carlo methods are the only viable method for using high dimensional particle type spaces. The accuracy of these methods is controlled by the number of computational particles used and the number of repeat runs with different random seeds. This can be computationally taxing under high rate conditions, such as those used in our recent study of industrial TiO_2 synthesis [4] because a large particle ensemble is required to resolve the polydisperse PSD and the surface structure of the particles evolves rapidly. In Monte Carlo methods, convergence to the exact solution is expected with increasing sample size. This can be demonstrated numerically [27, 36], and has been shown theoretically in several studies [7, 29, 40].

The stochastic approach has been refined with several techniques to reduce variance e.g. doubling [19] and mass flow algorithms [7] and weighted particle methods [12, 17, 31], and improve efficiency e.g. fictitious jumps/majorant kernels [8], linear process deferment algorithm [30]. Babovsky [3] proposes a scheme for studying gelation processes where, to reduce the chance of stochastic effects producing metastable states, two solution methods are used with: deterministic solution of the ODEs for particles of sizes smaller than N_1, stochastic solution for sizes between N_1 and N_2 and removal for larger particles (the gelled mass).

The purpose of this paper is to introduce a hybrid particle-number/particle (PN/P) model in which small particles are treated simply while large particles and aggregates are resolved with as much detail as possible. This split type space model is primarily intended to accommodate a detailed particle model when solving population balance equations with high rates of particle inception. Inception rates that produce a high number density of primary particles make it computationally challenging to resolve less abundant, larger particle aggregates, especially when particle surface processes such as heterogeneous reaction are also significant.

This paper is structured as follows: Two particle type sub-systems are defined using particle-number and detailed particle type space models respectively in Section 2. The final part of the section outlines the processes that transfer mass between the sub-systems. The population balance equations for formation and growth in both models are then developed in Section 3. The stochastic method used to advance the population balance equations is outlined in Section 4, and Section 5 presents numerical studies of the convergence and performance of the hybrid model compared to a standard particle model for a simplified TiO_2 test in various configurations.

2 Particle systems

Monte Carlo methods employ a finite ensemble of computational particles to model the diverse assortment of particles in the physical system. A computational particle P_i has a

distinct, possibly multivariate type, x_i, relating to the properties of the physical particle it represents. The particle type space describes all possible particles.

In this work, a hybrid particle-number/particle model is proposed wherein the particle type space is split and spherical particles below a certain threshold size are represented by a single internal coordinate (number of monomers) using a particle-number model. Particles larger than the threshold size and non-spherical aggregate particles formed by coagulation are modelled using a detailed particle model in order to resolve the complex information about their morphology. Particles are transferred from the particle-number type space to the particle type space when they grow larger than the threshold size or following coagulation events (Fig. 1).

If the particle model assumes that primary particles are spherical and composed of a single molecule type, and a large threshold size is feasible, the particle-number model does not introduce any approximation. The threshold size can be chosen to minimize the existence of spherical particles in the detailed particle system.

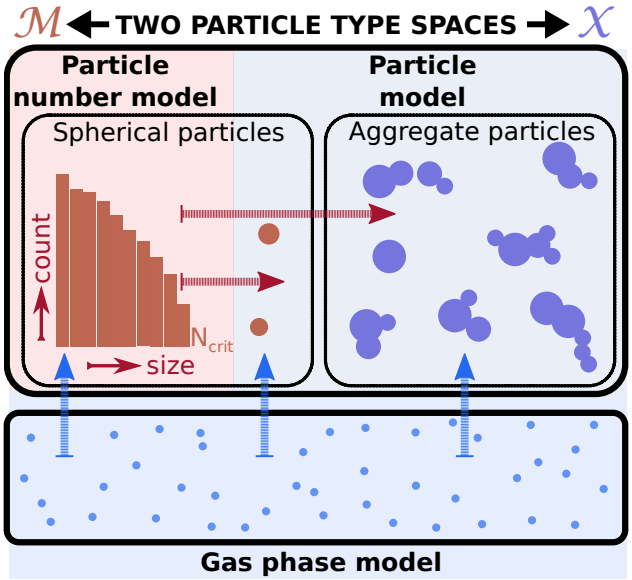

Figure 1: *Mass transfer from the gas phase to the particle systems by inception and surface reaction, and mass transfer from the particle-number model to the particle model by coagulation and surface growth beyond the threshold size (N_{thresh}).*

2.1 Space of small, spherical particles, $\mathcal{M}$

Let the particle type space consisting of small, spherical particles (primary particles) be defined as $\mathcal{M}$. Particles in this space have a single internal coordinate for number of monomers, with different sizes $i \in [1, N_{\text{thresh}}]$ where $i = 1$ is a single molecular unit and N_{thresh} is the size of the largest particle that is tracked by the particle-number model before transfer to the space of aggregate particles, $\mathcal{X}$. The particle-number (PN) system is written:

$$z_{\mathcal{M}}(t) = (x_1, \ldots, x_{N_{\text{thresh}}}),$$

where

$$x_i(t) \in \mathcal{M}, \quad i = 1, \ldots, N_{\text{thresh}}, \quad t \geq 0$$

and $N_i = N(x_i)$ is the number of particles that have type x_i. For continuous functions ϕ, the following convergence property can be maintained as the sample volume, V_{smp}, increases:

$$\int_{\mathcal{M}} \phi(x)\, n(t, dx) = \lim_{V_{\text{smp}} \to \infty} \frac{1}{V_{\text{smp}}} \sum_{i=1}^{N_{\text{thresh}}} N_i \phi(x_i(t)).$$

Here, $n(t,x)$ is the number density of particles with type x at time t and the concentration of particles with type $x_i \in \mathcal{M}$ is $N_i \cdot V_{\text{smp}}^{-1}$. $\mathcal{M}$ represents the type space efficiently as it requires only a vector in $\mathbb{R}^{N_{\text{thresh}}}$ to produce the PSD from the number of particles in each size class.

2.2 Space of large particles and aggregates, $\mathcal{X}$

Let $\mathcal{X}$ be the type space for spherical particles containing more than N_{thresh} monomers and all possible aggregate particles containing more than one primary particle. Particles in $\mathcal{X}$ need to be defined by both morphology and composition. A particle P_i is made up of an unordered list of primary particles, p_j, each of which is described by its chemical composition. The specific connectivity and extent of sintering between each neighbouring pair of primary particles is included in the particle description so that its morphology is known. The particle system is comprised of $N(t) \leq N_{\max}$ such particles (at time t):

$$z_{\mathcal{X}}(t) = \left(x_1, \ldots, x_{N(t)}\right),$$

where

$$x_i(t) \in \mathcal{X}, \quad i = 1, \ldots, N(t), \quad t \geq 0.$$

For continuous functions ϕ, the following convergence property is maintained where particles of type $x_i \in \mathcal{X}$ have concentration V_{smp}^{-1}:

$$\int_{\mathcal{X}} \phi(x)\, n(t, dx) = \lim_{V_{\text{smp}} \to \infty} \frac{1}{V_{\text{smp}}} \sum_{i=1}^{N(t)} \phi(x_i(t)).$$

The description of multivariate particle types x_i requires much more information for each particle; thus, a more sophisticated data structure is required to store each distinct particle separately [34].

2.3 Mass transfer between the particle systems

The concentration of particles of a given multivariate type $x \in (\mathcal{M} \cup \mathcal{X})$ can be evolved by the Smoluchowski coagulation equation [31], extended to include inception, surface growth and flow. Here, we consider flow in an ideal, constant volume, continuously stirred tank reactor (CSTR) (Eq. (1)).

$$\begin{aligned}\frac{\mathrm{d}n(t,x)}{\mathrm{d}t} =& I(x) + \frac{1}{2}\sum_{\substack{y,z\in(\mathcal{M}\cup\mathcal{X}):\\ y+z=x}} K(y,z)\,n(t,y)\,n(t,z) - \sum_{y\in(\mathcal{M}\cup\mathcal{X})} K(x,y)\,n(t,x)\,n(t,y) \\ &+ \sum_{\substack{y\in(\mathcal{M}\cup\mathcal{X}):\\ g_{\mathrm{SG}}(y)=x}} \beta_{\mathrm{SG}}(y)\,n(t,y) - \beta_{\mathrm{SG}}(x)\,n(t,x) + \frac{1}{\tau_{\mathrm{CSTR}}}\sum_{j=1}^{N_{\mathrm{in}}} f^{[j]}\left(n_{\mathrm{in}}^{[j]}(t,x) - n(t,x)\right)\end{aligned} \tag{1}$$

$I(x)$ is the rate of inception of particles of type x, $K(x,y)$ is the rate at which particles of type x coagulate with particles of type y, $\beta_{\mathrm{SG}}(y)$ is the rate of surface growth of particles of type y and $g_{\mathrm{SG}}(y)$ is the particle type that is produced by this surface growth, and τ_{CSTR} is the residence time in the CSTR. In the case of N_{in} inflow streams, $f^{[j]}$ is the volumetric feed fraction of the j^{th} stream.

Interaction with a gas phase system

The systems of interest in this work (i.e. flame synthesis) typically involve a gas phase precursor as well as several intermediate species, and formation and reaction processes in the gas phase must be described by a chemical mechanism. Particle synthesis follows from collision between gas phase species that results in a stable configuration of molecular units (inception). Particle growth also occurs due to the reaction of gas phase species on the particle surface (surface growth) and this creates a polydisperse primary particle size distribution.

Inception

Particle inception from the gas phase intermediates occurs at a rate, I, that depends on the gas phase concentrations and the temperature. The inception process only acts on the space of spherical primaries, $\mathcal{M}$, and not on the space of large particles, $\mathcal{X}$. In formulating the PBEs in the following section, we assume that a single monomer unit is the only incepting size; however, the description is transferable to any monomer index corresponding to a stable particle composition. Primary particles of type $x_1 \in \mathcal{M}$ are created and this is modelled by incrementing the count at index 1 in the particle-number model (Fig. 2).

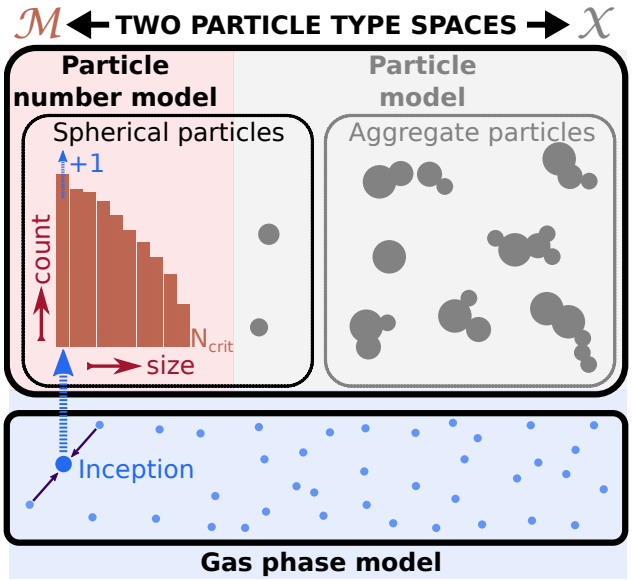

Figure 2: *Interaction between the gas phase and the particle-number system by inception of primary particles following gas phase collisions.*

Surface growth

All particles in the two type spaces can experience surface growth, at a rate, β_{SG}, that is dependent on the gas phase reactant concentrations and temperature, and the particle surface area. Surface growth results in a change in particle type according to the surface growth function, g_{SG}, with the following effects:

1. A particle described by the particle-number model with type $x_i \in \mathcal{M}$ is transformed to type $x_j = g_{\mathrm{SG}}(x_i)$, $i < j$. If the new size is still in $\mathcal{M}$, i.e. $j \leq N_{\mathrm{thresh}}$, the indices i and j are altered accordingly (Fig. 3, solid horizontal arrows).

2. If the new size exceeds the threshold size, i.e. $j > N_{\mathrm{thresh}}$, the particle is transferred to the detailed particle model, by creation of a new particle with type $x_j \in \mathcal{X}$ (Fig. 3, curved horizontal arrow).

3. Particles of type $x \in \mathcal{X}$, are transformed to larger type $y = g_{\mathrm{SG}}(x)$, $y \in \mathcal{X}$ (Fig. 3, dashed arrows).

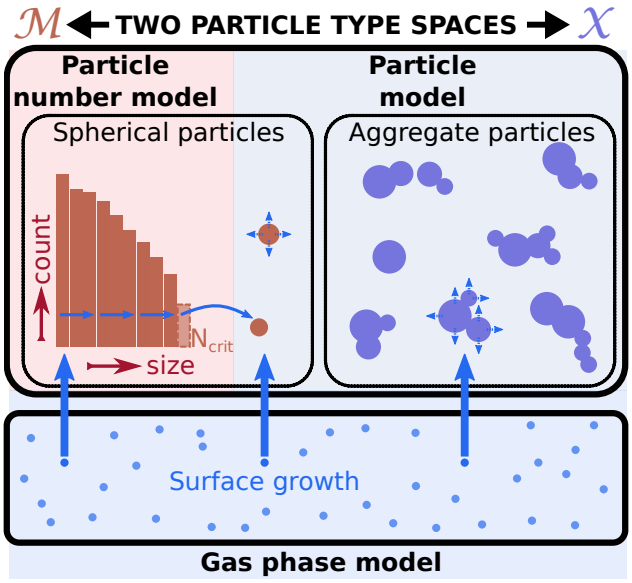

Figure 3: *Interaction between the gas phase and both particle systems by surface reaction (surface reaction beyond the threshold size N_{thresh} in the particle-number model causes transfer of particles to the particle model).*

Coagulation

Coagulation events can occur between any two particles across both type spaces $(\mathcal{M} \cup \mathcal{X})$. This transfers particles from the particle-number model (space $\mathcal{M}$) to the detailed particle model (space $\mathcal{X}$) (Fig. 4). Coagulation between two particle-number model particles forms a new aggregate in the particle model (this process acts as a source term for the particle model) and reduces the number of particle-number particles by two. Coagulation between two particle model particles reduces by one the number of particles in the particle model system. Coagulation between one particle from each space reduces the number of particles in the particle-number model by one. The PN particle can be attached to the coagulating particle model particle, conserving the count in the particle model.

The coagulation operator $\mathcal{K}$ acts on $(\mathcal{M} \cup \mathcal{X})^2$ and produces particles in $\mathcal{X}$. The symmetric coagulation kernel for each particle pair is $K(x,y)$ where $x, y \in (\mathcal{M} \cup \mathcal{X})$ and the total rate, R_{coag}, is:

$$
\begin{aligned}
R_{\text{coag}} &= \frac{1}{2V_{\text{smp}}} \iint_{(\mathcal{M}\cup\mathcal{X})^2} K(x,y)\, n(dx)\, n(dy) \\
&= \frac{1}{V_{\text{smp}}} \left[\frac{1}{2} \sum_{\substack{i=1 \\ x_i \in \mathcal{X}}}^{N(t)} \sum_{\substack{j=1;j\neq i \\ x_j \in \mathcal{X}}}^{N(t)} K(x_i,x_j) + \sum_{\substack{i=1 \\ x_i \in \mathcal{X}}}^{N(t)} \sum_{\substack{j=1 \\ x_j \in \mathcal{M}}}^{N_{\text{thresh}}} K(x_i,x_j) N_j + \frac{1}{2} \sum_{\substack{i=1 \\ x_i \in \mathcal{M}}}^{N_{\text{thresh}}} \sum_{\substack{j=1;(N_i<2 \iff j\neq i) \\ x_j \in \mathcal{M}}}^{N_{\text{thresh}}} K(x_i,x_j) N_i N_j \right].
\end{aligned}
\tag{2}
$$

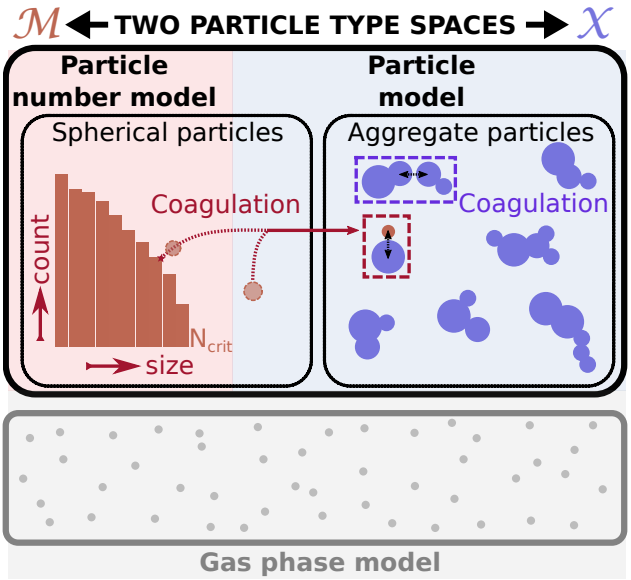

Figure 4: *Interaction between the particle systems by coagulation.*

Inflow

In a CSTR with particles in the inflow streams, particle inflow occurs with rate τ_{CSTR}^{-1} and particles can be added to both spaces with the following effects:

1. If $x_{\text{in}} = x_i \in \mathcal{M}$, the number of particles at the i^{th} index of the particle-number model is incremented: $N_i \leftarrow N_i + 1$, $i \in [1, N_{\text{thresh}}]$.
2. If $x_{\text{in}} \in \mathcal{X}$, a new particle with type x_{in} is added to the detailed particle system i.e. $z_{\mathcal{X}}(t) \leftarrow \{z_{\mathcal{X}}(t), P(x_{\text{in}})\}$.

Outflow

In a CSTR, particle outflow occurs with rate τ_{CSTR}^{-1} and particles can be removed from either particle system.

1. If $x_{\text{out}} = x_i \in \mathcal{M}$, the number of particles at the i^{th} index of the particle-number model is decremented: $N_i \leftarrow N_i - 1$, $i \in [1, N_{\text{thresh}}]$.
2. If $x_{\text{out}} \in \mathcal{X}$, the particle $P(x_{\text{out}})$ is removed from the detailed particle system i.e. $z_{\mathcal{X}}(t) \leftarrow \{z_{\mathcal{X}}(t) \setminus P(x_{\text{out}})\}$.

3 Population balance equations

Population balance equations can be formed for the number density $n(x)$ of particles of each type, $x \in \mathcal{M}$ and $x \in \mathcal{X}$. Let $\mathcal{I}$, $\mathcal{K}$, $\mathcal{S}$, $\mathcal{F}^{\text{in}}$ and $\mathcal{F}^{\text{out}}$ in Eqs. (3)-(5) be the inception, co-

agulation, surface growth, inflow and outflow operators respectively and let the subscript on the operator denote the relevant type space(s) involved in each case.

For $x_1 \in \mathcal{M}$:

$$\begin{aligned}
\frac{\mathrm{d}n_1}{\mathrm{d}t} =& \mathcal{I}_{x_1\in\mathcal{M}} - \left(\mathcal{K}_{x_1\in\mathcal{M}\leftrightarrow\mathcal{X}} + \mathcal{K}_{x_1\in\mathcal{M}\leftrightarrow\mathcal{M}}\right) - \mathcal{S}_{x_1\in\mathcal{M}} + \left(\mathcal{F}^{\text{in}}_{x_1\in\mathcal{M}} - \mathcal{F}^{\text{out}}_{x_1\in\mathcal{M}}\right) \\
\frac{\mathrm{d}n\left(x_1\right)}{\mathrm{d}t} =& I\left(x_1\right) - \sum_{\substack{j=1 \\ x_j\in\mathcal{X}}}^{N(t)} K\left(x_1,x_j\right) n\left(x_1\right) n\left(x_j\right) - \sum_{\substack{j=1;(N_1<2 \iff j\neq 1) \\ x_j\in\mathcal{M}}}^{N_{\text{thresh}}} K\left(x_1,x_j\right) n\left(x_1\right) n\left(x_j\right) \\
& - \beta_{\text{SG}}\left(x_1\right) n\left(x_1\right) + \frac{1}{\tau_{\text{CSTR}}} \sum_{j=1}^{N_{\text{in}}} f^{[j]} \left(n^{[j]}_{\text{in}}\left(x_1\right) - n\left(x_1\right)\right).
\end{aligned} \tag{3}$$

For $x_i \in \mathcal{M}$, $i = \{2,3,\ldots,N_{\text{thresh}}\}$:

$$\begin{aligned}
\frac{\mathrm{d}n_i}{\mathrm{d}t} =& -\left(\mathcal{K}_{x_i\in\mathcal{M}\leftrightarrow\mathcal{X}} + \mathcal{K}_{x_i\in\mathcal{M}\leftrightarrow\mathcal{M}}\right) + \left(\mathcal{S}_{\mathcal{M}} - \mathcal{S}_{x_i\in\mathcal{M}\cup\mathcal{X}}\right) + \left(\mathcal{F}^{\text{in}}_{x_i\in\mathcal{M}} - \mathcal{F}^{\text{out}}_{x_i\in\mathcal{M}}\right) \\
\frac{\mathrm{d}n\left(x_i\right)}{\mathrm{d}t} =& -\sum_{\substack{j=1 \\ x_j\in\mathcal{X}}}^{N(t)} K\left(x_i,x_j\right) n\left(x_i\right) n\left(x_j\right) - \sum_{\substack{j=1;(N_i<2 \iff j\neq i) \\ x_j\in\mathcal{M}}}^{N_{\text{thresh}}} K\left(x_i,x_j\right) n\left(x_i\right) n\left(x_j\right) \\
& - \beta_{\text{SG}}\left(x_i\right) n\left(x_i\right) + \sum_{\substack{j=1 \\ x_j\in\mathcal{M}}}^{i-1} \beta_{\text{SG}}\left(x_j\right) n\left(x_j\right) \mathbb{1}_{g_{\text{SG}}(x_j)=x_i} + \frac{1}{\tau_{\text{CSTR}}} \sum_{j=1}^{N_{\text{in}}} f^{[j]} \left(n^{[j]}_{\text{in}}\left(x_i\right) - n\left(x_i\right)\right).
\end{aligned} \tag{4}$$

For $x_i \in \mathcal{X}$, $i = \{1,2,\ldots,N(t)\}$:

$$\begin{aligned}
\frac{\mathrm{d}n_i}{\mathrm{d}t} =& \left(\mathcal{K}_{\mathcal{M}\leftrightarrow\mathcal{M}} + \mathcal{K}_{\mathcal{X}\leftrightarrow\mathcal{M}} + \mathcal{K}_{\mathcal{X}\leftrightarrow\mathcal{X}} - \mathcal{K}_{x_i\in\mathcal{X}\leftrightarrow\mathcal{M}} - \mathcal{K}_{x_i\in\mathcal{X}\leftrightarrow\mathcal{X}}\right) + \left(\mathcal{S}_{\mathcal{M}\cup\mathcal{X}} - \mathcal{S}_{x_i\in\mathcal{X}}\right) + \left(\mathcal{F}^{\text{in}}_{x_i\in\mathcal{X}} - \mathcal{F}^{\text{out}}_{x_i\in\mathcal{X}}\right) \\
\frac{\mathrm{d}n\left(x_i\right)}{\mathrm{d}t} =& \beta_{\text{SG}}\left(x_{\text{thresh}}\right) n\left(x_{\text{thresh}}\right) \mathbb{1}_{g_{\text{SG}}(x_{\text{thresh}})=x_i} \\
& - \sum_{\substack{j=1;j\neq i \\ x_j\in\mathcal{X}}}^{N(t)} K\left(x_i,x_j\right) n\left(x_i\right) n\left(x_j\right) - \sum_{\substack{j=1 \\ x_j\in\mathcal{M}}}^{N_{\text{thresh}}} K\left(x_i,x_j\right) n\left(x_i\right) n\left(x_j\right) \\
& + \frac{1}{2} \sum_{\substack{j=1 \\ x_j\in\mathcal{X}}}^{N(t)} \sum_{\substack{k=1;k\neq j \\ x_k\in\mathcal{X}}}^{N(t)} K\left(x_j,x_k\right) n\left(x_j\right) n\left(x_k\right) \mathbb{1}_{x_j+x_k=x_i} + \sum_{\substack{j=1 \\ x_j\in\mathcal{M}}}^{N_{\text{thresh}}} \sum_{\substack{k=1 \\ x_k\in\mathcal{X}}}^{N(t)} K\left(x_j,x_k\right) n\left(x_j\right) n\left(x_k\right) \mathbb{1}_{x_j+x_k=x_i} \\
& + \frac{1}{2} \sum_{\substack{j=1 \\ x_j\in\mathcal{M}}}^{N_{\text{thresh}}} \sum_{\substack{k=1;(N_j<2 \iff k\neq j) \\ x_k\in\mathcal{M}}}^{N_{\text{thresh}}} K\left(x_j,x_k\right) n\left(x_j\right) n\left(x_k\right) \mathbb{1}_{x_j+x_k=x_i} + \sum_{\substack{j=1 \\ x_j\in\mathcal{X}}}^{i-1} \beta_{\text{SG}}\left(x_j\right) n\left(x_j\right) \mathbb{1}_{g_{\text{SG}}(x_j)=x_i} \\
& - \beta_{\text{SG}}\left(x_i\right) n\left(x_i\right) + \frac{1}{\tau_{\text{CSTR}}} \sum_{j=1}^{N_{\text{in}}} f^{[j]} \left(n^{[j]}_{\text{in}}\left(x_i\right) - n\left(x_i\right)\right).
\end{aligned} \tag{5}$$

4 Stochastic numerical method

Strang operator splitting is used to couple the solution of the gas phase chemistry using an ODE solver and the solution of the particle population balance equations using a stochastic method in which the different events are performed probabilistically. This approach has been described elsewhere [5, 36] but is adapted here to handle the interaction between the two type space models (Alg. B.1).

In $\mathcal{M}$, the properties (mass, diameter etc.) corresponding to each size index in the particle-number space are stored at the simulation outset and just the total particle numbers at each index i.e.

$$N_i,\, i = 1, \ldots, N_{\text{thresh}}$$

and the property sums i.e.

$$\xi\left(z_{\mathcal{M}}\right) = \sum_{i=1}^{N_{\text{thresh}}} N_i \xi_i$$

are updated at runtime.

The gas phase chemistry is first updated for half a time step, after which a direct simulation algorithm (DSA) is used to advance the particle population balance equations (Eqs. (3)-(5)) for a full time step, over a number of smaller splitting steps. Each splitting step involves repeatedly sampling a waiting time from an exponential distribution defined by the total process rate, choosing a stochastic formation or growth event according to their relative rates and updating the relevant particle system to reflect this event (Alg. B.2).

If the selected process is inception, the particle-number model is adjusted by incrementing the count of particles at the index corresponding to the number of monomers in the incepting particle i.e.

$$N_1 \leftarrow N_1 + 1,$$

and the cached property sums for the particle-number system are updated i.e.

$$\xi\left(z_{\mathcal{M}}\left(t\right)\right) \leftarrow \xi\left(z_{\mathcal{M}}\left(t\right)\right) + \xi_1.$$

If the selected process is coagulation, a particle pair $\left(P_i, P_j\right)$ is selected using kernel-specific selection criteria. If a particle is selected from the particle-number class ($P_i \in \mathcal{M}$), the index corresponding to its monomer count is decremented i.e.

$$N_i \leftarrow N_i - 1,$$

and the cached property sums are updated i.e.

$$\xi\left(z_{\mathcal{M}}\left(t\right)\right) \leftarrow \xi\left(z_{\mathcal{M}}\left(t\right)\right) - \xi_i.$$

A new particle is created by cloning the i^{th} particle from the pre-initialised particle-number list. If both particles are selected from the particle-number system, the first is added to the ensemble at this stage:

$$z_{\mathcal{X}}\left(t\right) \leftarrow \left\{z_{\mathcal{X}}\left(t\right), P_i\right\}$$

and the second coagulates with it.

Particle outflow and surface updates are performed after each splitting step. The number of particles expected to leave the system over this time is sample from a Poisson distribution with rate parameter $1/\tau_{\text{CSTR}}$ and particles are removed by uniform selection followed by decreasing the particle-number count ($x_{\text{out}} \in \mathcal{M}$) or deletion ($x_{\text{out}} \in \mathcal{X}$).

The surface growth and sintering of adjacent primary particles is performed using a linear process deferment algorithm (LPDA). This defers the particle processes that occur independently for each particle and performs them either at the end of the splitting step, or during the step if the particle is selected for coagulation. This algorithm was introduced by Patterson et al. [30] to improve computational efficiency by reducing the number of times per step the algorithm halts to perform stochastic events. The particle-number counts are updated for surface growth in a second LPDA-type sub-scheme (Alg. B.3). This loops over all particle indices and computes the surface area dependent growth rate, samples the number of monomers to add from a Poisson distribution using this rate parameter, and uses this to determine a new index, which is incremented accordingly.

$$\begin{aligned} n_{\text{add,index}} &\sim \text{Poi}\left(\beta_{\text{SG}}\left(A_{\text{index}}\right)\right) \\ \text{newIndex} &\leftarrow \left(\text{index} + n_{\text{add,index}}\right). \end{aligned}$$

If the new index is larger than the threshold size, new particles are created and transferred to the detailed particle system.

4.1 Selecting particles according to their properties

Two particle selection processes are of interest. Uniform selection is used to choose particles to remove in outflow events, and a pair of particles to collide with a constant coagulation kernel. For more realistic coagulation kernels, selection of a pair of particles might depend on properties of the respective particles for example in the majorant proposed for the transition regime coagulation kernel (Table A.1), coagulation between small particles and large particles is often favoured. The selection algorithm is outlined in more detail in Algorithm B.4.

Random uniform selection

For the particle-number model with $x_i \in \mathcal{M}$, the index i of the selected particle is selected such that:

$$\mathbb{P}(\text{index} = i) = \frac{N_i}{\sum_{i=1}^{N_{\text{thresh}}} N_i}. \qquad \forall i \in \{1, \ldots, N_{\text{thresh}}\} \tag{6}$$

For the detailed particle model with $x_i \in \mathcal{X}$, particles $P(x_i)$ are selected such that:

$$\mathbb{P}(P_i) = \frac{1}{N(t)}. \qquad \forall i \in \{1, \ldots, N(t)\} \tag{7}$$

Selection according to particle properties

Let ξ be a property of the particles that is defined for both type spaces e.g. mass or diameter. For the particle-number model with $x_i \in \mathcal{M}$, the index i of the selected particle is determined using the property ξ as a weighting such that:

$$\mathbb{P}(\text{index} = i) = \frac{N_i \xi_i}{\sum_{j=1}^{N_{\text{thresh}}} N_j \xi_j}. \qquad \forall i \in \{1, \ldots, N_{\text{thresh}}\} \tag{8}$$

For the detailed particle model with $x_i \in \mathcal{X}$, particles $P(x_i)$ are selected using the property ξ as a weighting such that:

$$\mathbb{P}(P_i) = \frac{\xi(P_i)}{\sum_{j=1}^{N(t)} \xi(P_j)}. \qquad \forall i \in \{1, \ldots, N(t)\} \tag{9}$$

5 Numerical studies

5.1 Comparison with single particle type space model

The performance of the hybrid approach is compared with a single particle type space model in which the discrete ensemble describes the full type space, and primary particles are represented by stochastic entities in the ensemble alongside aggregate particles. The latter has been the standard approach for detailed population balance models to date [4, 25, 37]. Titanium dioxide (TiO_2) is taken as the particulate species and the gas phase mechanism of West et al. [41, 43] is used, although simplified artificial rates are used for easier analysis of the model behaviour. The TiO_2 system is of industrial interest; however modelling efforts are hindered by the computational cost of high process rates under industrially relevant conditions. The performance is assessed by comparative convergence behaviour (the double type space should not affect the solution since the particle-number indices fully encode the particle space at the level of primary particles defined by monomer count), solver time savings, and reduction in required ensemble size.

Test cases

Two test cases are considered, a batch reactor and a continuously stirred tank reactor (CSTR). A spherical particle model is used in the first case and a detailed model is used in the second case. Both reactors are constant volume, at 1200 K and 4 bar (absolute). Their residence times are 6 ms and 10 ms respectively. Time steps of 0.01 ms and 0.1 ms are used respectively, with 10 splitting steps per step (convergence with decreasing splitting step was studied by Shekar et al. [36]).

A constant inception rate is used, with the inception particle size taken to be 0.49 nm (2 TiO_2 units). Thus the particle-number model will always have zero particles at index 1. In the first case, the coagulation rate is constant $K = \tilde{K}$, and in the second case, a transition regime coagulation kernel $K = K^{\text{tr}}$ is used (Appendix A). The surface growth reaction adds TiO_2 units to the particle surface and the rate depends on surface area only,

$$\beta_{\text{SG}}(P_i) = \frac{\tilde{\beta}}{N_{\text{A}}} \cdot A(P_i), \forall (P_i) \in \mathcal{M} \cup \mathcal{X}.$$

Convergence tests

For given property ξ, a simulation with M timesteps, L repeat runs and a maximum ensemble size of $N_{\max}$ has mean value $\mu_\xi^{(N_{\max},L)}(t_k)$ at time t_k, $k \in [1,M]$(10)

$$\mu_\xi^{(N_{\max},L)}(t_k) = \frac{1}{L}\sum_{l=1}^{L} \xi^{(N_{\max},l)}(t_k), \tag{10}$$

and standard deviation $\sigma_\xi^{(N_{\max},L)}(t_k)$ at time t_k, $k \in [1,M]$ (11)

$$\sigma_\xi^{(N_{\max},L)}(t_k) = \sqrt{\frac{1}{L}\sum_{l=1}^{L}\left(\xi^{(N_{\max},l)}(t_k)\right)^2 - \left(\mu_\xi^{(N_{\max},L)}(t_k)\right)^2}. \tag{11}$$

The statistical error can be used to assess the random error in repeat simulations. The average relative statistical error at a given confidence level (here 99.9%, thus $\alpha_{0.999} = 3.29$) can be computed across all time steps (12)

$$\overline{\varepsilon}_{\text{stat},\xi}^{(N_{\max},L)} = \frac{1}{M}\sum_{k=1}^{M} \frac{\alpha_{0.999}}{\sqrt{L}} \cdot \frac{\sigma_\xi^{(N_{\max},L)}(t_k)}{\mu_\xi^{(N_{\max},L)}(t_k)}. \tag{12}$$

The average relative total error can be used to assess the relative difference compared to a true solution ξ^*. Here, the 'true' solution is approximated by the solution with $N_{\max} = 2^{18}$ (13) and the convergence study is performed for $N_{\max} \in \{2^6, 2^7, \ldots, 2^{17}\}$.

$$\overline{\varepsilon}_{\text{total},\xi}^{(N_{\max},L)} = \frac{1}{M}\sum_{k=1}^{M}\frac{\left|\mu_{\xi}^{(N_{\max},L)}(t_k) - \xi^*(t_k)\right|}{\xi^*(t_k)} \tag{13}$$

The properties used to illustrate convergence behaviour in this work include particle number concentration, $M_0(t)$, (14); the particle mass concentration and higher order moments of the particle mass concentration, $M_k(t)$, $k \in \{1,2,3\}$, (15); and the average particle collision diameter, d_c, (16) which is a measure of average particle size and is an example of a property that is of importance in applications.

$$M_0 = \frac{N(z_{\mathcal{M}}(t)) + N(z_{\mathcal{X}}(t))}{V_{\text{smp}}} \tag{14}$$

$$M_k = \frac{\sum_{i=1}^{N_{\text{thresh}}} m_i^k N_i + \sum_{i=1}^{N(z_{\mathcal{X}}(t))} (m(P_i))^k}{V_{\text{smp}}} \tag{15}$$

$$d_c(P_i) = \frac{6V_i}{A_i}(N_{\text{pri},i})^{\frac{1}{1.8}} \tag{16}$$

Solver time

All tests were run on one Intel Xeon E5-2640 CPU (2.40 GHz) of a 40 processor node with 200 GB RAM, running Red Hat Enterprise Linux version 7.2.

Case 1: constant rates batch reactor with spherical particle model

The constant rates case with spherical particle model is used to demonstrate proof of concept – under trivial constant rate conditions, the particle-number/particle model matches the convergence behaviour of the particle model (Figs. 5 and 6). The average relative error is compared with a single run of the particle model with $N_{\max} = 2^{18}$. The convergence tests were performed with $I = 10^{16}\ \text{cm}^{-3}\cdot\text{s}^{-1}$, $\tilde{\beta} = 10^{24}\ \text{cm}^{-5}\cdot\text{s}^{-1}$ and $\tilde{K} = 1.5\times10^{-15}\ \text{cm}^{-3}\cdot\text{s}^{-1}$.

The spherical particle model assumes each coagulation event is followed by instant coalescence to form a larger, spherical particle, so both type spaces hold the same information; however it should be possible to store/update this information more efficiently in a vector than a discrete ensemble. Surface growth events are performed once per particle since particles are not comprised of distinct primaries and choice of particles for coagulation and outflow is done by random selection. Thus the opportunities for improving run time with the PN/P model are limited; however, as expected it is more economical, especially for large ensembles (Fig. 7).

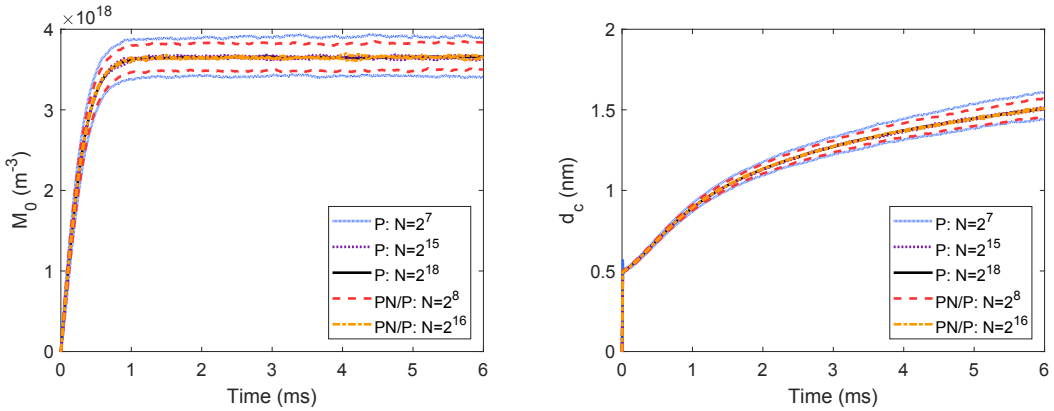

(a) Number density (b) Collision diameter

Figure 5: *Convergence study maintaining $N_{max} \times L = 2^{18}$ – the solid black line is the high fidelity solution and one standard deviation above and below the mean are shown as dotted lines for odd (particle model) and dashed lines for even (particle-number/particle model with $N_{thresh} = 10^2$) powers of 2 (case 1).*

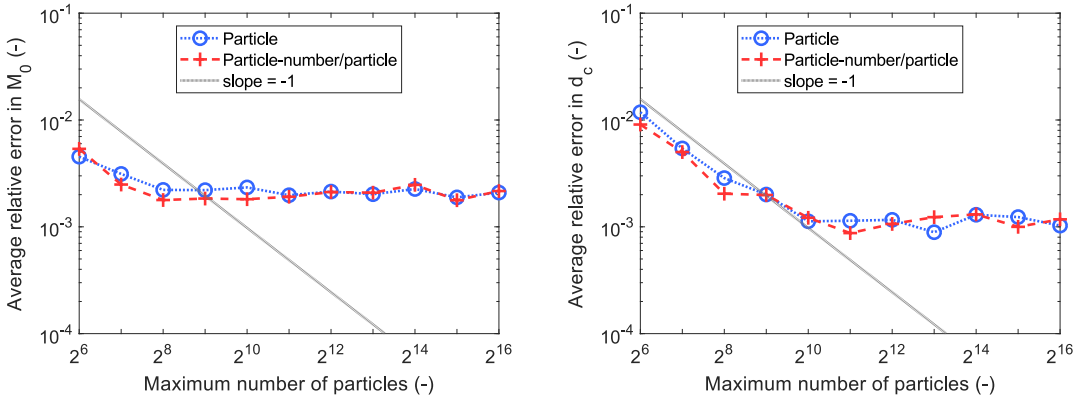

(a) Number density (total) (b) Particle diameter (total)

Figure 6: *Convergence study maintaining $N_{max} \times L = 2^{18}$ – average relative total error of the particle model and particle-number/particle model ($N_{thresh} = 10^2$) compared to the high fidelity solution (case 1 conditions).*

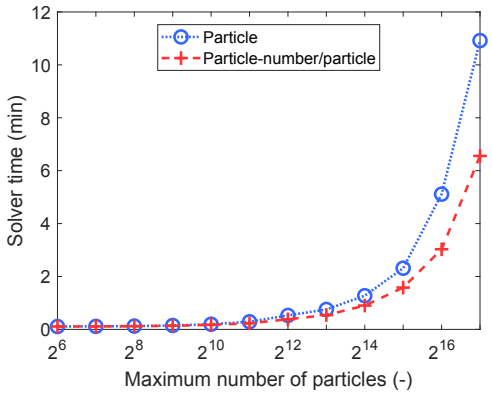

Figure 7: *Solver time comparison maintaining $N_{max} \times L = 2^{17}$ for the pure particle model and the particle-number/particle model with $N_{thresh} = 10^2$ (case 1 conditions).*

Case 2: transition kernel CSTR with detailed particle model

The transition coagulation kernel is chosen because it is relevant to real synthesis conditions and depends on the properties of each particle which makes its evaluation more costly. Particles are chosen for coagulation events according to individual property-dependent rates (Table A.1). The transition kernel has the form

$$K^{\mathrm{tr}}(P_i,P_j) = \frac{K^{\mathrm{sf}}(P_i,P_j)\,K^{\mathrm{fm}}(P_i,P_j)}{K^{\mathrm{sf}}(P_i,P_j)+K^{\mathrm{fm}}(P_i,P_j)}, \forall (P_i,P_j) \in \mathcal{M} \cup \mathcal{X}. \tag{17}$$

K^{sf} and K^{fm} are defined in Appendix A. Surface growth is performed on every primary particle in each aggregate. The average relative error is compared with ten runs of the particle model with $N_{\max} = 2^{18}$. The convergence tests were performed with $I = 10^{12}$ cm$^{-3} \cdot$ s^{-1} and $\tilde{\beta} = 10^{24}$ cm$^{-5} \cdot$ s^{-1}.

Here, the rates are more complicated, yet the simulation with the two type space models converges on the same properties as the single type space approach (Figs. 8 and 9); slight discrepancies between the PN/P model and the 'true' solution with the particle model exist due to differences in the ordering of particles (i.e. a list in increasing size order vs. an unordered list of particles as formed could influence which particle is selected in Alg. B.4).

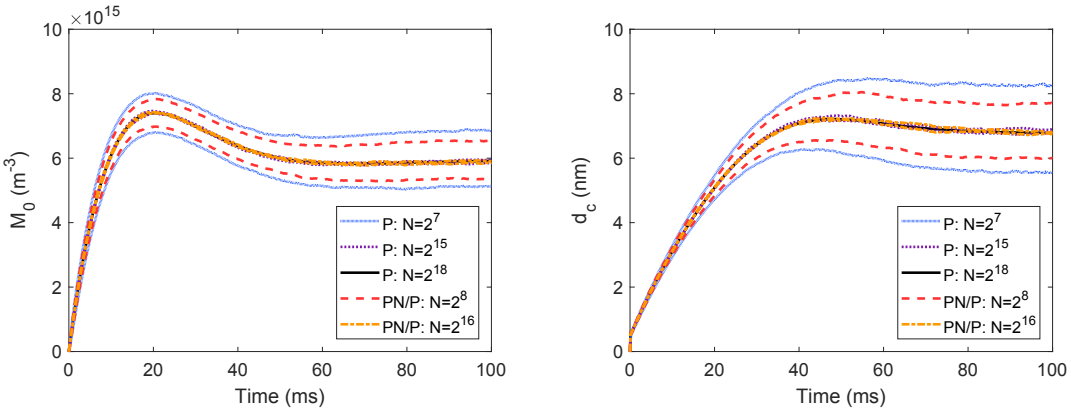

(a) Number density (b) Collision diameter

Figure 8: *Convergence study maintaining $N_{max} \times L = 2^{18}$ – the solid black line is the high fidelity solution and one standard deviation above and below the mean are shown as dotted lines for odd (particle model) and dashed lines for even (particle-number/particle model with $N_{thresh} = 10^4$) powers of 2 (case 2 conditions).*

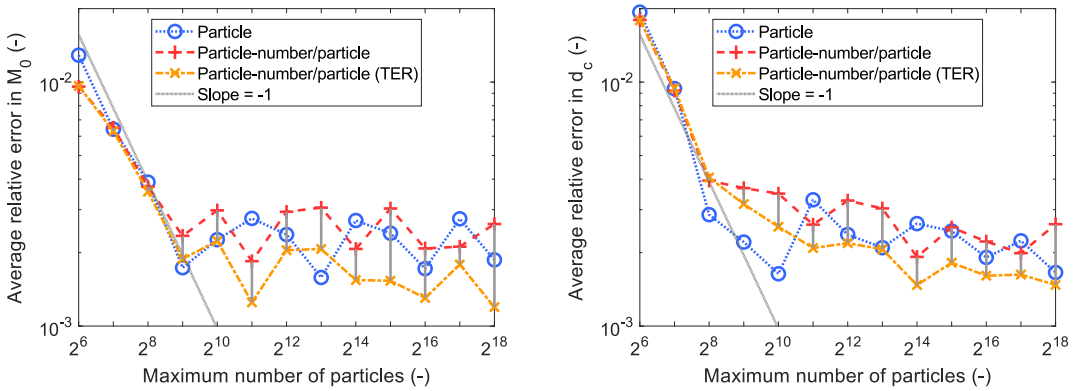

(a) Number density (total) (b) Particle diameter (total)

Figure 9: *Convergence study maintaining $N_{max} \times L = 2^{18}$ – average relative total error of the particle model, particle-number/particle model ($N_{thresh} = 10^4$), and PN/P model with time equivalent runs (TER) compared to the high fidelity solution (case 2 conditions).*

Differences in run time (Fig. 10) are more significant than in the study with the spherical particle model. This is especially noticeable for large ensembles where updates to the particle-number list are much more efficient than updates to distinct particles and a speed up of approximately 50% is observed for the ensembles with greater than 10^5 particles (Fig. 10(b)). For small ensembles, the PN/P model is more efficient in a narrower range of threshold values. In general, a threshold of $N_{\text{thresh}} = 10^4$ was found to work well for the current conditions.

The reduced solver time is advantageous if CPU time is constrained; however the main benefit is that this allows an increase in the sample volume in the PN/P model, i.e. use of a time equivalent sample volume (TESV, Table 1 column 3), or an increase in the number of repeat runs in the PN/P model, i.e. use of time equivalent runs (TER, Table 1 column 4), to gain additional accuracy for comparable CPU cost (Fig. 8, solid vertical lines illustrate reduced error with additional repeats for same computational cost).

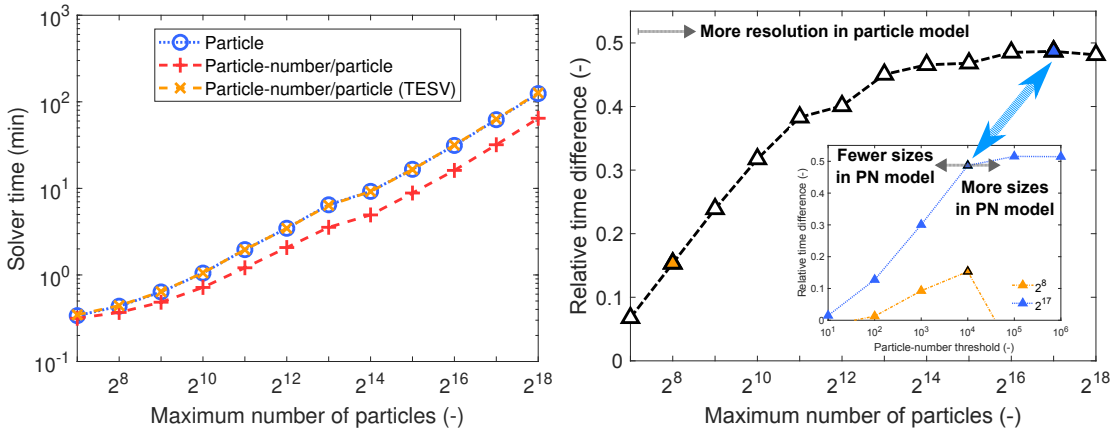

(a) Solver times

(b) Relative solver time difference

Figure 10: *Solver times and relative time difference maintaining $N_{max} \times L = 2^{18}$ for pure particle model and particle-number(PN)/particle model with inset showing effect of threshold value N_{thresh} (case 2 conditions).*

Table 1: *Sample volume increase or additional repeats that can be achieved with solver time savings gained from PN/P model with $N_{thresh} = 10^4$ (case 2 conditions).*

Ensemble size, $N_{\max}$	Repeats, L	Sample volume increase	Time equivalent repeats
2^7	2048	1.67	2196
2^8	1024	1.67	1209
2^9	512	1.70	672
2^{10}	256	1.74	375
2^{11}	128	1.81	207
2^{12}	64	1.88	107
2^{13}	32	1.90	58
2^{14}	16	1.95	30
2^{15}	8	1.97	15
2^{16}	4	2.00	8
2^{17}	2	2.00	4
2^{18}	1	2.03	2

The PN/P model removes most of the solo primary particles from the discrete particle ensemble, which allows the discrete ensemble to be used almost exclusively to resolve more

complicated aggregate particles for the same computational cost and ensemble memory overhead by using a larger sample volume, as shown in the simulated imaging pictures in Fig. 11. This ensures that maximum utility is obtained from the detailed particle model without 'wasting' ensemble space and time on structurally simple particles.

An alternative approach is to maintain a more economical memory foot-print by initialising a smaller ensemble for tracking fewer distinct particles. This could be useful for systems that have an initial burst of particle inception due to high concentration of the gas phase precursor yielding a high initial number density. In such a system, doubling and contraction algorithms are often necessary with a discrete ensemble since demand for capacity varies with time. The particle-number list can store arbitrarily many incepting particles so the ensemble can be customized to the size required to store aggregates only.

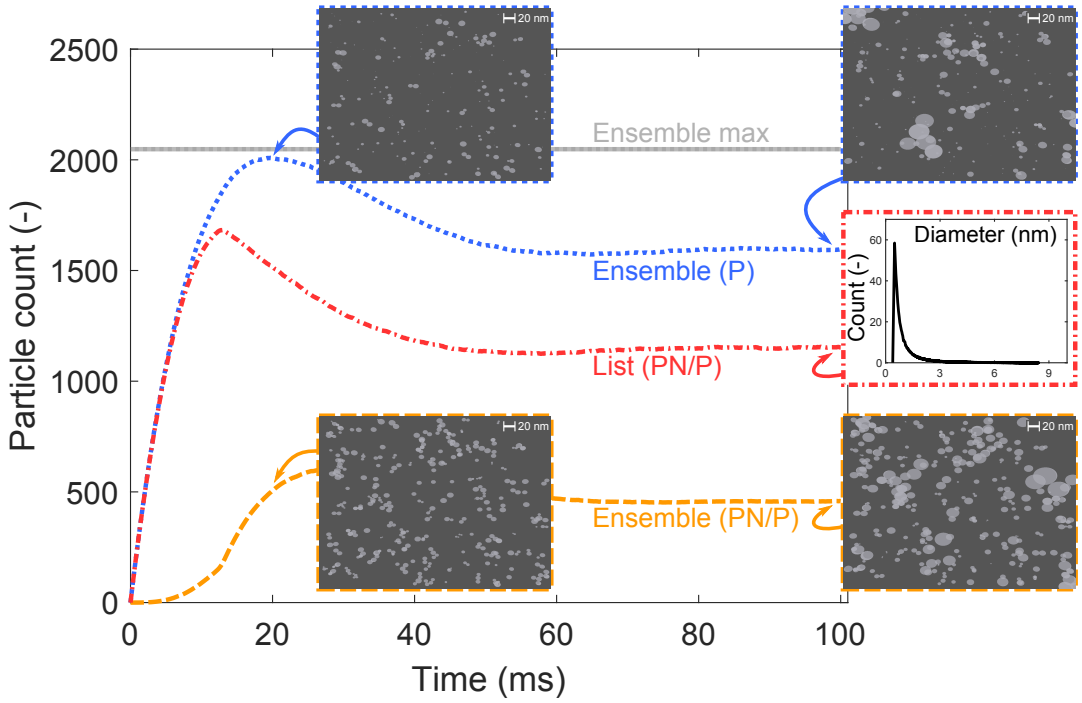

Figure 11: *Particle counts in the ensemble and particle-number list for particle model (P) and particle-number/particle model (PN/P), with inset simulated SEMs of 200 tracked ensemble particles at 20 ms and 100 ms (scale bar shows 20 nm) for* $N_{max} = 2^{11}$ *and* $N_{thresh} = 10^4$ *(PN/P with runtime equivalent sample volume).*

The effect of exceeding the ensemble capacity is illustrated further in Fig. 12. With a single discrete particle model, increasing the sample volume by a factor of three from the previous conditions results in contractions in the interval $t \in [4.8, 20]$ ms (shown in Fig. 12(a) with a horizontal arrow) because there is no space for new particles in the discrete ensemble so inceptions are accommodated by randomly removing an existing particle from the ensemble and scaling the sample volume to preserve the particle number density. With the hybrid type space model, particle inceptions contribute to the particle-number space, $\mathcal{M}$, instead of being added to the ensemble space, $\mathcal{X}$. This list storage (shown in Fig. 12(a) with a vertical arrow) prevents the ensemble from flooding; thus no

particles are removed.

Particle removal randomizes the system when the particles are polydisperse. This can be seen in Fig. 12(b): tripling the sample volume significantly increases the total error for the particle model (*cf.* packed circle pattern labelled "P: V_{smp}" and checkerboard pattern labelled "P: $3V_{\text{smp}}$") whereas it reduces the total error for the hybrid model (*cf.* wave pattern labelled "PN/P: V_{smp}" and stripe pattern labelled "PN/P: $3V_{\text{smp}}$") due to the increased statistical significance of events in the larger sample volume.

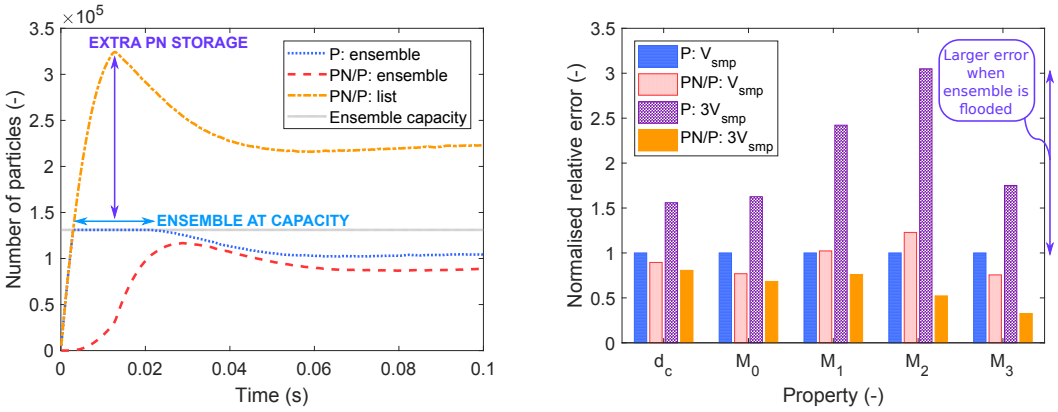

(a) Particle counts in $3V_{\text{smp}}$ case

(b) Average error in converged solutions

Figure 12: *Effect of exceeding ensemble capacity with $N_{max} = 2^{17}$ – normalised total relative error in: particle model; PN/P model ($N_{thresh} = 10^4$); particle model with triple sample volume; and PN/P model with triple sample volume (case 2 conditions).*

5.2 Performance of Pn/P model in different rate regimes

Performance of the PN/P model is assessed in different rate regimes using the conditions in Table 2, for the CSTR from case 2 with a transition regime coagulation kernel and a detailed particle model for the aggregate type space.

Table 2: *Inception and surface reaction rate constants used in rate study.*

Process	Units	Rate constants			
Inception	$[\text{cm}^{-3} \cdot \text{s}^{-1}]$	1×10^{6}	1×10^{9}	1×10^{12}	1×10^{13}
Surface reaction	$[\text{cm}^{-5} \cdot \text{s}^{-1}]$	1×10^{18}	1×10^{21}	1×10^{24}	

The process rates are coupled since the coagulation rate increases quadratically with number density and depends on properties of the particles such as diameter. To simplify the analysis, the average ratio of the rates is used in Figs. 13 and 14:

$$\text{Mean rate ratio (inception:coagulation)} = \frac{1}{M}\sum_{m=1}^{M}\frac{R_{\text{inception}}(t_m)}{R_{\text{coagulation}}(t_m)}$$

$$\text{Mean rate ratio (surface reaction:coagulation)} = \frac{1}{M}\sum_{m=1}^{M}\frac{R_{\text{surface reaction}}(t_m)}{R_{\text{coagulation}}(t_m)}.$$

The mean count ratio is used to assess the utility of the particle-number list for storing particles and refers to the average particle-number count divided by the average ensemble count:

$$\text{Mean count ratio} = \frac{1}{M}\sum_{m=1}^{M}\frac{N(z_{\mathcal{M}}(t_m))}{N(z_{\mathcal{X}}(t_m))}.$$

The combined particle-number/(detailed)particle model offers considerable performance advantages over the use of a single detailed particle model for conditions that result in a large number of solo primary particles (when inception dominates coagulation). In these cases, most of the particles in the system can be stored in the particle-number list, significantly reducing the ensemble size requirements (Fig. 13(a)). Conditions with high surface growth and similar coagulation and inception rates do not see significant solver time advantage with the PN/P model (Fig. 13(b)) because the coagulation processes produce large aggregates and the surface updates for these complex structures dominate the solver time; however, the there are still significantly many primary particles in the particle-number list under these conditions and the option to use a smaller particle ensemble could still be attractive due to improved memory efficiency. Future work should consider methods for mitigating the aggregate update cost.

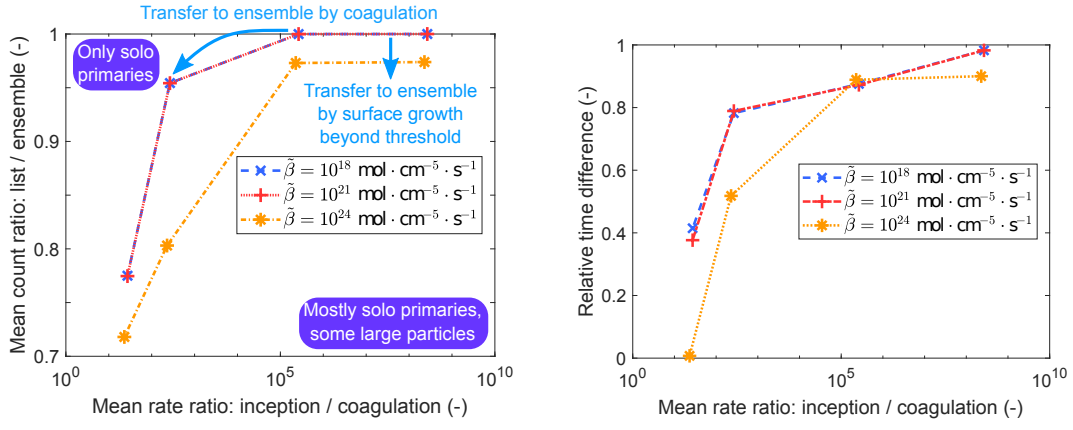

(a) Ratio of particles

(b) Solver time difference

Figure 13: *Ratio of particles in the particle-number list to particles in the ensemble in the PN/P model and corresponding solver time difference for different ratios of inception rate to coagulation rate (using threshold $N_{thresh} = 2^{17}$).*

When the surface growth rate is very high, primary particles grow rapidly and are pulled out of the particle-number system into the particle system unless a large threshold value is used to store the primaries in the particle-number system for as long as possible (Fig. 14(a)). The number density of very large primaries becomes lower with increasing index (Fig. 14(b)), so use of a high threshold (e.g. $N_{\text{thresh}} = 10^4$) achieves limited additional particle storage; however, since the updates to the particle-number model are comparatively cheap even for large thresholds, it is reasonable to use a large threshold to avoid wasting ensemble space on single primary particles.

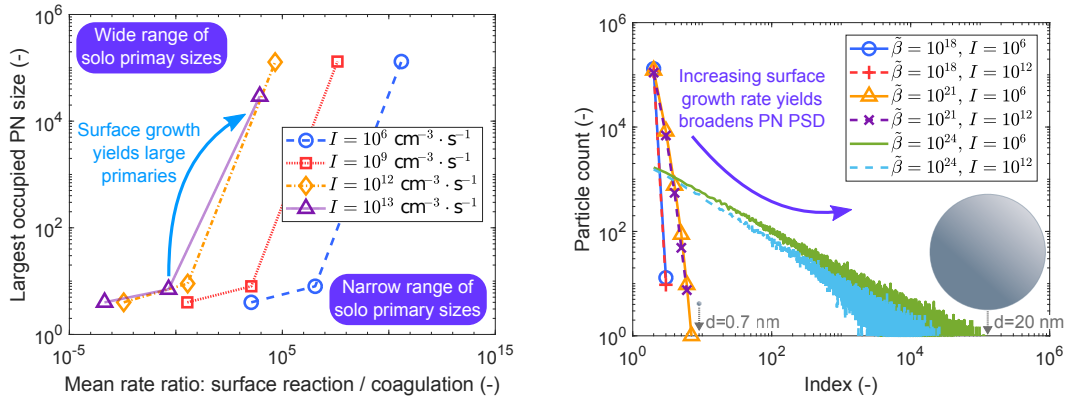

(a) Largest nonzero PN index

(b) Counts for each PN index

Figure 14: *Largest occupied particle-number (PN) size and PN size distributions at t_f for different ratios of surface reaction rate to coagulation rate (using threshold $N_{thresh} = 2^{17}$).*

6 Conclusion

A hybrid particle-number/particle model was presented for reducing the computational requirements of population balance simulations under certain high rate conditions. When the inception rate is at least an order of magnitude higher than the coagulation rate, single primary particles are formed significantly faster than they collide with other particles, leading to a system dominated by single primaries. The particle-number type space model is introduced here to track the distribution of these primaries up to a given threshold. Primaries that coagulate or grow to sizes above the threshold are transferred to a detailed particle type space model in order to resolve their morphology.

Under low surface growth conditions, the required threshold to store all primaries is small because the range of primary sizes is narrow; however, under high surface growth conditions, it is advantageous to use a larger threshold in order to accommodate the wider range of primary sizes and benefit from the more efficient update structure of the particle-number list. The proposed hybrid model is less effective when the coagulation rate is very high, because the computational complexity associated with very large aggregate particles dominates the solver time. The hybrid scheme offers two main benefits.

1. It can be up to 50% faster than a single detailed particle type space model when the surface growth rate is high and the surface updates to ensemble particles are expensive. This speed-up can be traded for a larger sample volume to achieve a greater statistical accuracy for comparable cost and memory. One possible application where this would make a really significant improvement is if particle-particle heat transfer effects were included and the surface updates for each particle were even more costly.

2. When the inception/coagulation ratio is large, most particles can be stored in the particle-number list, reducing the size of particle ensemble required to resolve the aggregate particles. This smaller ensemble has a lower memory footprint. One possible application would be in coupling to computational fluid dynamics simulations where the memory and computational cost associated with large ensembles would be prohibitive. This also assists tailoring the ensemble to the size needed to store aggregate particles, by avoiding initial periods of high inception when the precursor concentration is high, without resorting to contraction and doubling algorithms.

A number of adaptations are possible for different systems.

1. If the internal co-ordinate is not 'quantized' (multiples of a monomer subunit), the indexing can be converted to sections of larger width at the cost of introducing some approximation error within the sections.

2. For more efficiency, it might be assumed that collisions between small particles result in instant coalescence, allowing these collisions to be performed in the particle-number model. This could be controlled using the sintering rate to determine where this assumption is near to the actual behaviour.

3. Weighted particle methods such as described by Patterson et al. [31] could be employed to reduce the number of particles injected to the ensemble by surface growth beyond the threshold.

Acknowledgements

This project is partly funded by the National Research Foundation (NRF), Prime Minister's Office, Singapore under its Campus for Research Excellence and Technological Enterprise (CREATE) programme. The authors would also like to thank Venator for financial support.

References

[1] J. Akroyd, A. J. Smith, L. R. McGlashan, and M. Kraft. Numerical investigation of DQMoM-IEM as a turbulent reaction closure. *Chemical Engineering Science*, 65 (6):1915–1924, 2010. ISSN 00092509. doi:10.1016/j.ces.2009.11.010.

[2] J. Akroyd, A. J. Smith, R. Shirley, L. R. McGlashan, and M. Kraft. A coupled CFD-population balance approach for nanoparticle synthesis in turbulent reacting flows. *Chemical Engineering Science*, 66(17):3792–3805, 2011. ISSN 00092509. doi:10.1016/j.ces.2011.05.006.

[3] H. Babovsky. A hybrid numerical scheme for aerosol dynamics. In *Numerical Mathematics and Advanced Applications*, pages 425–432. Springer, 2008. ISBN 978-3-540-69776-3. doi:0.1007/978-3-540-69777-0.

[4] A. Boje, J. Akroyd, S. Sutcliffe, J. Edwards, and M. Kraft. Detailed population balance modelling of TiO_2 synthesis in an industrial reactor. *Chemical Engineering Science*, 164:219–231, 2017. ISSN 00092509. doi:10.1016/j.ces.2017.02.019.

[5] M. S. Celnik, R. I. A. Patterson, M. Kraft, and W. Wagner. Coupling a stochastic soot population balance to gas-phase chemistry using operator splitting. *Combustion and Flame*, 148(3):158–176, 2007. ISSN 00102180. doi:10.1016/j.combustflame.2006.10.007.

[6] M. S. Celnik, M. Sander, A. Raj, R. H. West, and M. Kraft. Modelling soot formation in a premixed flame using an aromatic-site soot model and an improved oxidation rate. *Proceedings of the Combustion Institute*, 32(1):639–646, 2009. ISSN 15407489. doi:10.1016/j.proci.2008.06.062.

[7] A. Eibeck and W. Wagner. Stochastic Particle Approximations for Smoluchoski's Coagualtion Equation. *The Annals of Applied Probability*, 11(4):1137–1165, 2001. ISSN 10505164. doi:10.1214/aoap/1015345398.

[8] A. Eibeck and W. Wagner. Stochastic interacting particle systems and nonlinear kinetic equations. *The Annals of Applied Probability*, 13(3):845–889, 2003. ISSN 1050-5164. doi:10.1214/aoap/1060202829.

[9] M. Frenklach. Method of moments with interpolative closure. *Chemical Engineering Science*, 57(12):2229–2239, 2002. ISSN 00092509. doi:10.1016/S0009-2509(02)00113-6.

[10] M. Frenklach and S. J. Harris. Aerosol dynamics modeling using the method of moments. *Journal of Colloid and Interface Science*, 118(1):252–261, 1987. ISSN 00219797. doi:10.1016/0021-9797(87)90454-1.

[11] M. J. Hounslow, R. L. Ryall, and V. R. Marshall. A discretized population balance for nucleation, growth, and aggregation. *AIChE Journal*, 34(11):1821–1832, 1988. ISSN 0001-1541. doi:10.1002/aic.690341108.

[12] G. Kotalczyk and F. Kruis. A Monte Carlo method for the simulation of coagulation and nucleation based on weighted particles and the concepts of stochastic resolution and merging. *Journal of Computational Physics*, 340:276–296, 2017. ISSN 00219991. doi:10.1016/j.jcp.2017.03.041.

[13] M. Kraft. Modelling of Particulate Processes. *KONA Powder and Particle Journal*, 23:18–35, 2005. ISSN 0288-4534. doi:10.14356/kona.2005007.

[14] S. Kumar and D. Ramkrishna. On the solution of population balance equations by discretization–I. A fixed pivot technique. *Chemical Engineering Science*, 51(8): 1311–1332, 1996. ISSN 00092509. doi:10.1016/0009-2509(96)88489-2.

[15] S. Kumar and D. Ramkrishna. On the solution of population balance equations by discretization–II. A moving pivot technique. *Chemical Engineering Science*, 51(8): 1333–1342, 1996. ISSN 00092509. doi:10.1016/0009-2509(95)00355-X.

[16] S. Kumar and D. Ramkrishna. On the solution of population balance equations by discretization–III. Nucleation, growth and aggregation of particles. *Chemical Engineering Science*, 52(24):4659–4679, 1997. ISSN 00092509. doi:10.1016/S0009-2509(97)00307-2.

[17] K. F. Lee, R. I. A. Patterson, W. Wagner, and M. Kraft. Stochastic weighted particle methods for population balance equations with coagulation, fragmentation and spatial inhomogeneity. *Journal of Computational Physics*, 303:1–18, 2015. ISSN 00219991. doi:10.1016/j.jcp.2015.09.031.

[18] C. Lindberg, J. Akroyd, and M. Kraft. Developing breakage models relating morphological data to the milling behaviour of flame synthesised titania particles. *Chemical Engineering Science*, 166, 2017. ISSN 00092509. doi:10.1016/j.ces.2017.03.016.

[19] A. Maisels, F. Einar Kruis, and H. Fissan. Direct simulation Monte Carlo for simultaneous nucleation, coagulation, and surface growth in dispersed systems. *Chemical Engineering Science*, 59(11):2231–2239, 2004. ISSN 00092509. doi:10.1016/j.ces.2004.02.015.

[20] M. Y. Manuputty, J. Akroyd, S. Mosbach, and M. Kraft. Modelling TiO_2 formation in a stagnation flame using method of moments with interpolative closure. *Combustion and Flame*, 178:135–147, 2017. ISSN 00102180. doi:10.1016/j.combustflame.2017.01.005.

[21] D. L. Marchisio and R. O. Fox. Solution of population balance equations using the direct quadrature method of moments. *Journal of Aerosol Science*, 36(1):43–73, 2005. ISSN 00218502. doi:10.1016/j.jaerosci.2004.07.009.

[22] D. L. Marchisio, J. T. Pikturna, R. O. Fox, R. D. Vigil, and A. A. Barresi. Quadrature method of moments for population-balance equations. *AIChE Journal*, 49(5):1266–1276, 2003. ISSN 00011541. doi:10.1002/aic.690490517.

[23] R. McGraw. Description of aerosol dynamics by the quadrature method of moments. *Aerosol Science and Technology*, 27(2):255–265, 1997. ISSN 15217388. doi:10.1080/02786829708965471.

[24] W. J. Menz and M. Kraft. The Suitability of Particle Models in Capturing Aggregate Structure and Polydispersity. *Aerosol Science and Technology*, 47(7):734–745, 2013. ISSN 0278-6826. doi:10.1080/02786826.2013.788244.

[25] W. J. Menz and M. Kraft. A new model for silicon nanoparticle synthesis. *Combustion and Flame*, 160(5):947–958, 2013. ISSN 00102180. doi:10.1016/j.combustflame.2013.01.014.

[26] W. J. Menz, R. I. A. Patterson, W. Wagner, and M. Kraft. Application of stochastic weighted algorithms to a multidimensional silica particle model. *Journal of Computational Physics*, 248:221–234, 2013. ISSN 00219991. doi:10.1016/j.jcp.2013.04.010.

[27] W. J. Menz, J. Akroyd, and M. Kraft. Stochastic solution of population balance equations for reactor networks. *Journal of Computational Physics*, 256:615–629, 2014. ISSN 00219991. doi:10.1016/j.jcp.2013.09.021.

[28] H. K. Park and K. Y. Park. Control of Particle Morphology and Size in Vapor-Phase Synthesis of Titania, Silica and Alumina Nanoparticles. *KONA Powder and Particle Journal*, 32(32):85–101, 2015. ISSN 0288-4534. doi:10.14356/kona.2015018.

[29] R. I. A. Patterson. Convergence of Stochastic Particle Systems Undergoing Advection and Coagulation. *Stochastic Analysis and Applications*, 31(5):800–829, 2013. ISSN 0736-2994. doi:10.1080/07362994.2013.817245.

[30] R. I. A. Patterson, J. Singh, M. Balthasar, M. Kraft, and J. R. Norris. The Linear Process Deferment Algorithm: A new technique for solving population balance equations. *SIAM Journal on Scientific Computing*, 28(1):303–320, 2006. ISSN 1064-8275. doi:10.1137/040618953.

[31] R. I. A. Patterson, W. Wagner, and M. Kraft. Stochastic weighted particle methods for population balance equations. *Journal of Computational Physics*, 230(19):7456–7472, 2011. ISSN 00219991. doi:10.1016/j.jcp.2011.06.011.

[32] S. E. Pratsinis and P. T. Spicer. Competition between gas phase and surface oxidation of $TiCl_4$ during synthesis of TiO_2 particles. *Chemical Engineering Science*, 53(10):1861–1868, 1998. ISSN 00092509. doi:10.1016/S0009-2509(98)00026-8.

[33] A. D. Randolph and M. A. Larson. *Theory of particulate processes: analysis and techniques of continuous crystallization*. Academic Press, San Diego, 2nd ed. edition, 1988. ISBN 0125796528.

[34] M. Sander, R. H. West, M. S. Celnik, and M. Kraft. A Detailed Model for the Sintering of Polydispersed Nanoparticle Agglomerates. *Aerosol Science and Technology*, 43(10):978–989, 2009. ISSN 0278-6826. doi:10.1080/02786820903092416.

[35] M. Sander, R. I. A. Patterson, A. Braumann, A. Raj, and M. Kraft. Developing the PAH-PP soot particle model using process informatics and uncertainty propagation. *Proceedings of the Combustion Institute*, 33(1):675–683, 2011. ISSN 15407489. doi:10.1016/j.proci.2010.06.156.

[36] S. Shekar, W. J. Menz, A. J. Smith, M. Kraft, and W. Wagner. On a multivariate population balance model to describe the structure and composition of silica nanoparticles. *Computers & Chemical Engineering*, 43:130–147, 2012. ISSN 00981354. doi:10.1016/j.compchemeng.2012.04.010.

[37] S. Shekar, A. J. Smith, W. J. Menz, M. Sander, and M. Kraft. A multidimensional population balance model to describe the aerosol synthesis of silica nanoparticles. *Journal of Aerosol Science*, 44:83–98, 2012. ISSN 00218502. doi:10.1016/j.jaerosci.2011.09.004.

[38] S. Tsantilis and S. E. Pratsinis. Evolution of primary and aggregate particle-size distributions by coagulation and sintering. *AIChE Journal*, 46(2):407–415, 2000. ISSN 00011541. doi:10.1002/aic.690460218.

[39] H. Wang. Formation of nascent soot and other condensed-phase materials in flames. *Proceedings of the Combustion Institute*, 33(1):41–67, 2011. ISSN 15407489. doi:10.1016/j.proci.2010.09.009.

[40] C. G. Wells. A stochastic approximation scheme and convergence theorem for particle interactions with perfectly reflecting boundary conditions. *Monte Carlo Methods and Applications*, 12(3):291–342, 2006. ISSN 0929-9629. doi:10.1515/156939606778705182.

[41] R. H. West, G. J. O. Beran, W. H. Green, and M. Kraft. First-Principles Thermochemistry for the Production of TiO_2 from $TiCl_4$. *The Journal of Physical Chemistry A*, 111(18):3560–3565, 2007. ISSN 1089-5639. doi:10.1021/jp0661950.

[42] R. H. West, M. S. Celnik, O. R. Inderwildi, M. Kraft, G. J. O. Beran, and W. H. Green. Toward a Comprehensive Model of the Synthesis of TiO_2 Particles from $TiCl_4$. *Industrial & Engineering Chemistry Research*, 46(19):6147–6156, 2007. ISSN 0888-5885. doi:10.1021/ie0706414.

[43] R. H. West, R. A. Shirley, M. Kraft, C. F. Goldsmith, and W. H. Green. A detailed kinetic model for combustion synthesis of titania from $TiCl_4$. *Combustion and Flame*, 156(9):1764–1770, 2009. ISSN 00102180. doi:10.1016/j.combustflame.2009.04.011.

[44] S. Wu, E. K. Yapp, J. Akroyd, S. Mosbach, R. Xu, W. Yang, and M. Kraft. A moment projection method for population balance dynamics with a shrinkage term. *Journal of Computational Physics*, 330:960–980, 2017. ISSN 00219991. doi:10.1016/j.jcp.2016.10.030.

[45] Y. Xiong and S. E. Pratsinis. Formation of agglomerate particles by coagulation and sintering – Part I. A two-dimensional solution of the population balance equation. *Journal of Aerosol Science*, 24(3):283–300, 1993. ISSN 00218502. doi:10.1016/0021-8502(93)90003-R.

[46] E. K. Yapp, D. Chen, J. Akroyd, S. Mosbach, M. Kraft, J. Camacho, and H. Wang. Numerical simulation and parametric sensitivity study of particle size distributions in a burner-stabilised stagnation flame. *Combustion and Flame*, 162(6):2569–2581, 2015. ISSN 00102180. doi:10.1016/j.combustflame.2015.03.006.

Nomenclature

Upper-case Roman

A	Surface area	$[\mathrm{m}^2]$
C	Concentration	$[\mathrm{mol} \cdot \mathrm{m}^{-3}]$
I	Inception rate	$[\mathrm{mol} \cdot \mathrm{m}^{-3} \cdot \mathrm{s}^{-1}]$
K	General coagulation kernel	$[\mathrm{m}^{-3} \cdot \mathrm{s}^{-1}]$
$\tilde{K}$	Coagulation constant	
$\hat{K}$	Majorant coagulation kernel	
Kn	Knudsen number	
L	Number of repeat runs	
M	Number of time steps	
M_0	0^{th} number moment	$[\mathrm{m}^{-3}]$
N	Number	
N_A	Avogadro's constant	$[\mathrm{mol}^{-1}]$
P	Pressure	[Pa]
P	Particle	
Poi	Poisson distribution	
R	Rate	[process specific]
T	Temperature	[K]
U	Uniform distribution	
V	Volume	$[\mathrm{m}^3]$

Lower-case Roman

c	Constant	
d	Diameter	[nm]
f	Volumetric feed fraction	
g	Surface growth type-change function	
k_B	Boltzmann constant	$[\mathrm{J} \cdot \mathrm{K}^{-1}]$
m	Mass	[kg]
n	Particle number concentration	$[\mathrm{m}^{-3}]$
p	Primary particle	
t	Time	[s]
x	Particle type variable	
y	Particle type variable	
z	Particle system	

Lower-case Greek

α	Random variable	
β	Surface growth rate	$[\mathrm{m}^2 \cdot \mathrm{m}^{-3} \cdot \mathrm{s}^{-1}]$

$\tilde{\beta}$	Surface growth constant	
γ	Weighted random variable	
$\bar{\varepsilon}$	Average relative error	
μ	Viscosity	$[\mathrm{Pa}\cdot\mathrm{s}]$
μ_ξ	Mean value of property ξ	
ξ	Property	
ρ	Mass density	$[\mathrm{kg}\cdot\mathrm{m}^{-3}]$
σ_ξ	Standard deviation of property ξ	
τ	Residence time	[s]
ϕ	Arbitrary continuous function	

Superscripts

fm	Free molecular
in	inflow
out	Outflow
sf	Slip flow
tr	Transition
$*$	Denotes reference solution

Subscripts

c	Collision
coag	Coagulation
i	Index variable
in	inflow
inc	inception
j	Index variable
k	Index variable
max	Maximum
out	Outflow
pri	Primary particle
SG	Surface growth
smp	Sample
split	Splitting time
stat	Statistical
thresh	Threshold
tmp	Template
1	Denotes monomer size (first) index

Symbols

$\mathcal{F}$	Flow operator
$\mathcal{K}$	Coagulation operator

$\mathcal{I}$	Inception operator
$\mathcal{M}$	Small particle type space
$\mathbb{P}$	Mathematical probability
$\mathcal{S}$	Surface growth operator
$\mathcal{X}$	Large particle type space
$\mathbb{1}$	Indicator function
$\forall$	For all

Abbreviations

CFD	Computational fluid dynamics
CSTR	Continuous stirred tank reactor
DSA	Direct simulation algorithm
DQMOM	Direct quadrature method of moments
LPDA	Linear process deferment algorithm
MOMIC	Method of moments with interpolative closure
ODE	Ordinary differential equation
PBE	Population balance equation
PN/P	Particle-number/particle
PSD	Particle size distribution
DQMOM	Direct quadrature method of moments
QMOM	Quadrature method of moments
SWA	Stochastic weighted algorithm
SEM	Scanning electron microscopy
TER	Time-equivalent repeats
TESV	Time-equivalent sample volume

A Transition regime coagulation kernel

The transition kernel has the form

$$K^{\mathrm{tr}}(P_i,P_j)=\frac{K^{\mathrm{sf}}(P_i,P_j)\,K^{\mathrm{fm}}(P_i,P_j)}{K^{\mathrm{sf}}(P_i,P_j)+K^{\mathrm{fm}}(P_i,P_j)},\ \forall(P_i,P_j)\in\mathcal{M}\cup\mathcal{X}, \tag{A.1}$$

where K^{sf} and K^{fm} are the slip-flow and free-molecular kernels defined below in which in which m is the particle mass, k_{B} is the Boltzmann constant, P is the pressure, and Kn is the Knudsen number [36].

$$\begin{aligned}
K_{\mathrm{sf}}(P_i,P_j)&=\frac{2k_{\mathrm{B}}T}{3\mu}\left(\frac{1+1.257\mathrm{Kn}(P_i)}{d_{\mathrm{c}}(P_i)}+\frac{1+1.257\mathrm{Kn}(P_j)}{d_{\mathrm{c}}(P_j)}\right)(d_{\mathrm{c}}(P_i)+d_{\mathrm{c}}(P_j))\\
K_{\mathrm{fm}}(P_i,P_j)&=2.2\sqrt{\frac{\pi k_{\mathrm{B}}T}{2}\left(\frac{1}{m(P_i)}+\frac{1}{m(P_j)}\right)}(d_{\mathrm{c}}(P_i)+d_{\mathrm{c}}(P_j))^2\\
\mathrm{Kn}(P_i)&=4.74\times10^{-8}\frac{T}{Pd_{\mathrm{c}}(P_i)}
\end{aligned}$$

Majorant kernel techniques are used to reduce the computational complexity of evaluating the double summation over the particle space for the non-linear coagulation kernel. The technique used here is described by Patterson et al. [31] and Menz et al. [26]. The kernel K is bounded by a larger kernel $\hat{K}$ which is easier to evaluate. In order to achieve the correct coagulation behaviour, the majorant rate is used to compute the total coagulation rate R_{coag} (2); however individual coagulation events between particles P_i and P_j are only performed with probability $K_{ij}\cdot\hat{K}_{ij}^{-1}$.

The majorant used for the free-molecular kernel is

$$\hat{K}_{\mathrm{fm}}(P_i,P_j)=4.4\sqrt{\frac{\pi k_{\mathrm{B}}T}{2}}\left(\frac{1}{\sqrt{m(P_i)}}+\frac{1}{\sqrt{m(P_j)}}\right)\left(d_{\mathrm{c}}(P_i)^2+d_{\mathrm{c}}(P_j)^2\right). \tag{A.2}$$

Define

$$\beta_1=4.4\sqrt{\frac{\pi k_{\mathrm{B}}T}{2}}.$$

Then

$$\hat{K}_{\mathrm{fm}}(P_i,P_j)=\beta_1\left(\frac{d_{\mathrm{c}}(P_i)^2}{\sqrt{m(P_i)}}+\frac{d_{\mathrm{c}}(P_i)^2}{\sqrt{m(P_j)}}+\frac{d_{\mathrm{c}}(P_j)^2}{\sqrt{m(P_i)}}+\frac{d_{\mathrm{c}}(P_j)^2}{\sqrt{m(P_j)}}\right). \tag{A.3}$$

The slip-flow kernel does not require a majorant. Define

$$\beta_2 = \frac{2k_B T}{3\mu}$$
$$\beta_3 = 1.257 \times 4.74 \times 10^{-8} \frac{T}{P}.$$

Then

$$K_{sf}(P_i, P_j) = \beta_2 \left(2 + \frac{d_c(P_i)}{d_c(P_j)} + \frac{d_c(P_j)}{d_c(P_i)} + \beta_3 \left(\frac{1}{d_c(P_i)} + \frac{d_c(P_i)}{d_c(P_j)^2} + \frac{d_c(P_j)}{d_c(P_i)^2} + \frac{1}{d_c(P_j)} \right) \right). \tag{A.4}$$

By the techniques described in Patterson et al. [31], this yields the selection properties given in Table A.1 for particle pairs for coagulation.

Table A.1: *Particle properties used to choose coagulation pair (P_i, P_j) based on transition regime majorant kernel terms.*

Term	P_i	P_j
Free-molecular 1	Uniform	$d_c(P_j)^2 \cdot m(P_j)^{-0.5}$
Free-molecular 2	$d_c(P_i)^2$	$m(P_j)^{-0.5}$
Slip-flow 1	Uniform	Uniform
Slip-flow 2	$d_c(P_i)$	$d_c(P_j)^{-1}$
Slip-flow 3	Uniform	$d_c(P_j)^{-1}$
Slip-flow 4	$d_c(P_i)$	$d_c(P_j)^{-2}$

B Algorithms

Algorithm B.1: Operator-splitting algorithm with particle-number/particle model

Input: $\mathbf{C}(t_0)$, $T(t_0)$, $z_{\mathcal{X}}(t_0)$, $z_{\mathcal{M}}(t_0)$, d_{inc}, N_{thresh}, t_f.
Output: $\mathbf{C}(t_f)$, $T(t_f)$, $z_{\mathcal{X}}(t_f)$, $z_{\mathcal{M}}(t_f)$, $N(z_{\mathcal{M}}(t_f))$.
Set $t \leftarrow t_0$, $C \leftarrow C(t_0)$, $T \leftarrow T(t_0)$, $z_{\mathcal{X}} \leftarrow z_{\mathcal{X}}(t_0)$, $z_{\mathcal{M}} \leftarrow z_{\mathcal{M}}(t_0)$,$N_{\mathcal{M}} \leftarrow N(z_{\mathcal{M}}(t_0))$
$\Delta t = t_f - t_0$.
Solve gas phase ODEs for $\left[t, t+\frac{\Delta t}{2}\right]$: $\mathbf{C} \leftarrow C\left(t+\frac{\Delta t}{2}\right)$, $T \leftarrow T\left(t+\frac{\Delta t}{2}\right)$.
while $t < t_f$ **do**
  Calculate overall rates of non-deferred processes:

$$R_{\text{inception}} = I(\mathbf{C}, T); \quad R_{\text{coagulation}} = \mathcal{K}\left((\mathcal{X} \cup \mathcal{M})^2\right); \quad R_{\text{total}} = R_{\text{inception}} + R_{\text{coagulation}}.$$

  Adjust the maximum splitting time t_{split} given R_{total} and set $t_{\text{flow}} \leftarrow t$.
  while $t < t_{split}$ **do**
    Select a process and perform it using waiting time algorithm (Alg. B.2).
    Select number, n, of particles for outflow:

$$n \sim \text{Poi}\left(\frac{t - t_{\text{flow}}}{\tau}\left(\sum_{i=1}^{N_{\text{thresh}}} N_i + N(t)\right)\right).$$

    while $n > 0$ **do**
      Uniformly select a particle P_i (Alg. B.4) and set $n \leftarrow (n-1)$.
      if $P_i \in \mathcal{M}$ **then**

$$N_i \leftarrow (N_i - 1).$$

      else

$$z_{\mathcal{X}} \leftarrow z_{\mathcal{X}} \setminus P_i.$$

      end
    end
  end
  for $i = 1, \ldots, N(t)$ **do**
    Do surface growth update on P_i, sinter its primaries, update gas phase $\mathbf{C}$, T.
  end
  Adjust particle-number list $z_{\mathcal{M}}$ for surface growth (Alg. B.3).
end

Algorithm B.2: Waiting time algorithm with particle-number/particle model

Input: $\mathbf{C}(t_0)$, $T(t_0)$, $z_{\mathcal{X}}(t_0)$, $z_{\mathcal{M}}(t_0)$, d_{inc}, N_{thresh}, t_{split}.
Output: $\mathbf{C}(t_f)$, $T(t_f)$, $z_{\mathcal{X}}(t_f)$, $z_{\mathcal{M}}(t_f)$.
Set $t \leftarrow t_0$, $C \leftarrow C(t_0)$, $T \leftarrow T(t_0)$, $z_{\mathcal{X}} \leftarrow z_{\mathcal{X}}(t_0)$, $z_{\mathcal{M}} \leftarrow z_{\mathcal{M}}(t_0)$.
Calculate overall rates of non-deferred processes:

$$R_{\text{inception}} = I(\mathbf{C}, T); \quad R_{\text{coagulation}} = \mathcal{K}\left((\mathcal{X} \cup \mathcal{M})^2\right); \quad R_{\text{total}} = R_{\text{inception}} + R_{\text{coagulation}}.$$

Select a waiting time $\tau \sim \exp(R_{\text{total}})$.
if $t + \tau < t_{split}$ **then**
  Choose process $\in \{\text{inception, coagulation}\}$ using:

$$\mathbb{P}(\text{process}) = R_{\text{process}} \cdot {R_{\text{total}}}^{-1}.$$

  if *process* = *inception* **then**
    Update property sums for change in number of particles at index 1.

$$N_1 \leftarrow (N_1 + 1); \qquad N(z_{\mathcal{M}}) \leftarrow (N(z_{\mathcal{M}}) + 1).$$

    Update gas phase $\mathbf{C}$, T.
  else if *process* = *coagulation* **then**
    if $(N(z_{\mathcal{M}}) + N(z_{\mathcal{X}})) > 1$ **then**
      Pick $(P_i, P_j) \in (\mathcal{X} \cup \mathcal{M})$ (Alg. B.4) and allow coagulation with probability:

$$\mathbb{P}_{i,j} = K_{\text{tr}}(P_i, P_j) \cdot \hat{K}_{\text{tr}}(P_i, P_j)^{-1}.$$

      if *Coagulation allowed* **then**
        if $(P_k \in \mathcal{M}, k = \{i, j\})$ **then**
          Update property sums for change in number of particles at index k.

$$N_k \leftarrow (N_k - 1); \qquad N(z_{\mathcal{M}}) \leftarrow N(z_{\mathcal{M}}) - 1.$$

        end
        if $(P_i \in \mathcal{M}, P_j \in \mathcal{M})$ **then**
          Add P_i to ensemble:

$$z_{\mathcal{X}} \leftarrow \{z_{\mathcal{X}}, P_i\}; \qquad N(z_{\mathcal{X}}) \leftarrow (N(z_{\mathcal{X}}) + 1).$$

        end
        Perform coagulation $P_i \leftarrow (P_i + P_j)$.
      end
    end
  end
  Set $t \leftarrow (t + \tau)$.
else
  Set $t \leftarrow (t + t_{\text{split}})$.
end

Algorithm B.3: Update particle-number lists

Input: $\mathbf{C}(t)$, $T(t)$, $z_{\mathcal{X}}(t)$, $z_{\mathcal{M}}(t)$, N_{thresh}, t_f, template particle of size d_{thresh}: $P_{\text{thresh}}^{\text{tmp}}$.
Output: $\mathbf{C}(t_f)$, $T(t_f)$, $z_{\mathcal{M}}(t_f)$.
Set $n_{\text{add,total}} \leftarrow 0$.
Compute expected surface growth factor:

$$\tilde{\beta} \leftarrow \tilde{\beta}(\mathbf{C}, T)(t_f - t_0).$$

for $index = N_{thresh}, \ldots, 1$ **do**
  if $N_{index} > 0$ **then**
    Choose number of units to add from:

$$n_{\text{add,index}} \sim \text{Poi}\left(\tilde{\beta} A(P_{\text{index}})\right).$$

    Set newIndex $\leftarrow$ (index $+ n_{\text{add,index}}$).
    if $newIndex > index$ **then**
      Update $n_{\text{add,total}} \leftarrow (n_{\text{add,total}} + n_{\text{add,index}})$.
      if $newIndex \leq N_{thresh}$ **then**
        Update property sums for change in number at index, newIndex.
        Set $N_{\text{newIndex}} \leftarrow (N_{\text{newIndex}} + N_{\text{index}})$.
        Set $N_{\text{index}} \leftarrow 0$.
      else
        Update property sums for change in number at index.
        Update total particle number:

$$N(z_{\mathcal{M}}) \leftarrow (N(z_{\mathcal{M}}) - N_{\text{index}}).$$

        Set $N_{\text{index}} \leftarrow 0$.
        Copy template particle:

$$P_{\text{new}} \leftarrow P_{\text{thresh}}^{\text{tmp}}.$$

        Add (newIndex $- N_{\text{thresh}}$) monomers to P_{new}.
        for $j = 1, \ldots, N_{index}$ **do**
          Add particle to ensemble:

$$z_{\mathcal{X}} \leftarrow \{z_{\mathcal{X}}, P_{\text{new}}\}.$$

        end
      end
    end
  end
end
Update gas phase $\mathbf{C}$, T for $n_{\text{add,total}}$ surface growth events.

Algorithm B.4: Particle selection algorithm with particle-number/particle model

Input: $z_{\mathcal{X}}(t)$, $z_{\mathcal{M}}(t)$, selection criterion 'choose according to property ξ'.
Output: Selected particle P_i.
Define the sums of properties in each space (note these properties are cached):

$$\Sigma_{\mathcal{M}} \leftarrow \sum_{i=1}^{N_{\text{thresh}}} N_i \xi_i; \qquad \Sigma_{\mathcal{X}} \leftarrow \sum_{i=1}^{N(t)} \xi(P_i); \qquad \Sigma_{\text{total}} \leftarrow \Sigma_{\mathcal{M}} + \Sigma_{\mathcal{X}}.$$

Choose a uniform random number: $\alpha \sim \mathrm{U}(0,1)$.
Set $\gamma \leftarrow \alpha \Sigma_{\text{total}}$.
if $\gamma \leq \Sigma_{\mathcal{M}}$ **then**
    `/* Select index` i `from particle-number list` $z_{\mathcal{M}}$ `*/`
    $j \leftarrow 1$.
    while $j \leq N_{thresh}$ **do**
        if $\gamma \leq (N_j \xi_j)$ **then**
            $i \leftarrow j$.
        end
        else
            $\gamma \leftarrow (\gamma - N_j \xi_j)$.
            $j \leftarrow (j+1)$.
        end
    end
    Create the new particle P_i[a].
else
    `/* Select particle` P_i `from particle ensemble` $z_{\mathcal{X}}$ `*/`
    $\gamma \leftarrow \alpha \Sigma_{\text{total}} - \Sigma_{\mathcal{M}}$.
    $j \leftarrow 1$.
    while $j \leq N(t)$ **do**
        if $\gamma \leq \xi(P_j)$ **then**
            $i \leftarrow j$.
        end
        else
            $\gamma \leftarrow (\gamma - \xi(P_j))$.
            $j \leftarrow (j+1)$.
        end
    end
    Use the ensemble particle P_i.
end

[a] Clone the particle with index i from reference particle list